# Chemical and structural characterization of UICC crocidolite fibres from Koegas Mine, Northern Cape (South Africa)

Alessandro Pacella [1,*], Giovanni B. Andreozzi [1], Luca Nodari [2], Paolo Ballirano [1]

[1] Department of Earth Sciences, Sapienza University of Rome, Piazzale Aldo Moro 5, I-00185 Rome, Italy
[2] Institute of Condensed Matter Chemistry and Technologies for Energy (ICMATE), National Research Council of Italy (CNR), Corso Stati Uniti 4, 35127 Padova, Italy

## ARTICLE INFO

## ABSTRACT

In the present work we report the full structural and spectroscopic characterization of an UICC crocidolite standard sample, that is a fibrous riebeckite from Koegas Mine, Northern Cape (South Africa). The chemical composition was obtained by SEM-EDS and cation site partition was retrieved by complementing chemical, Mössbauer and X-ray powder diffraction data. Cell parameters, fractional coordinates, and site scattering for $M(1)$, $M(2)$, $M(3)$, $M(4)$ were refined using the Rietveld method.

The UICC crocidolite standard sample shows the chemical formula $^A Na_{0.026} {}^B Na_{2.000} {}^C (Fe^{2+}_{2.212} Fe^{3+}_{2.041} Mg_{0.747})_{\Sigma=5.000} {}^T (Si_{7.950} Al_{0.022})_{\Sigma=7.972} O_{22} {}^{O(3)}(OH)_2$, very close to that of the end-member riebeckite $^A \square {}^B Na_2 {}^C (Fe^{2+}_3 Fe^{3+}_2)_{\Sigma=5} {}^T Si_8 O_{22} {}^{O(3)}(OH)_2$, the major difference being the $Fe^{3+}/Fe_{tot}$ ratio of 0.48, slightly higher than the ideal ratio of 0.40. Cation site distribution of the UICC crocidolite standard sample is: $[Mg_{0.50} Fe^{3+}_{0.31} Fe^{2+}_{1.19}]_{\Sigma=2.00}$ at $M(1)$; $[Mg_{0.10} Fe^{3+}_{1.60} Fe^{2+}_{0.30}]_{\Sigma=2.00}$ at $M(2)$; $[Mg_{0.15} Fe^{3+}_{0.13} Fe^{2+}_{0.72}]_{\Sigma=1.00}$ at $M(3)$. Refined cell parameters are: $a$=9.73516(19) Å, $b$=18.0453(3) Å, $c$=5.32895(9) Å, $\beta$=103.5159(12) °, $V$=910.23(3) Å$^3$. Quantitative Phase Analysis indicates that 93.7(3) wt% of the sample consists of crocidolite, the remaining being distributed among five different phases including magnetite and quartz.

Keywords: asbestos; UICC crocidolite; Scanning Electron Microscopy with Energy Dispersive System (SEM-EDS); Mössbauer Spectroscopy; X-ray Powder Diffraction (XRPD), Rietveld method; surface reactivity.

## INTRODUCTION

Asbestos is a group of six naturally-occurring silicate including one fibrous serpentine (chrysotile) and five fibrous amphiboles (anthophyllite, tremolite, actinolite, riebeckite, and grunerite, with the last two commercially known as crocidolite and amosite, respectively). Asbestos has been widely used in the past in a number of industrial settings due to its high tensile strength, flexibility, electrical and thermal resistance, but today is banned in several countries, due to health risks posed by their inhalation (IARC, 2012). Indeed, despite an extraordinary research effort, the mechanism through which asbestos fibres may give rise to disease is not yet completely clear. Toxicological studies show that interactions between fibrous material and biological environment are strongly dependent on both the morphology and the crystal chemistry of mineral fibres (Stanton et al., 1981; Bonneau et al., 1986; Fubini, 1993, 1996; Gilmour et al., 1997). In particular, both the presence and structural coordination of surface iron are considered key factors in the toxicity of asbestos (Fubini and Mollo, 1995; Martra et al., 2003; Favero-Longo et al., 2005; Gazzano et al., 2005). Besides,

PM

the recent work of Andreozzi et al. (2017) showed that the amphibole asbestos (crocidolite and tremolite) fibre surface may undergo chemical modifications when in contact with fluids at physiological pH of 7.4, with consequent modification of the Fe topochemistry resulting in the modulation of the fibre reactivity. In particular, they showed that the radical production is dependent on specific surface Fe sites, occupied by either $Fe^{2+}$ or $Fe^{3+}$, with unsaturated coordinative valences. Furthermore, Andreozzi et al. (2017) highlighted a different behaviour of crocidolite with respect to tremolite in both dissolution and Fe speciation kinetics. Iron-rich crocidolite exhibited the fastest dissolution leading to a pronounced transfer of bulk Fe to the surface, with consequent formation of an armouring of Fe-rich nanoparticles. Iron-poor tremolite, on the contrary, showed a slow dissolution process with partial amorphisation of external layers and absence of armouring.

Although crocidolite (i.e., fibrous riebeckite) is the most studied type of asbestos from the toxicological point of view, only very few structural data are available in the scientific literature. The first structural refinement of a fibrous riebeckite from Bolivia was done by Whittaker (1949), indeed representing the first example of a crystal structure refinement of a fibrous amphibole. According to its formula, $(Na_{1.38}K_{0.13}Ca_{0.17}Mg_{0.25})$ $(Mg_{2.81}Fe^{3+}_{1.66}Fe^{2+}_{0.48}Al_{0.05})[Si_{7.94}Al_{0.06}O_{22}](OH)_2$, the investigated sample may be classified as a magnesio-riebeckite. The refined structure is very similar to that later reported by Hawthorne (1978) for fluoro-riebeckite and by Hawthorne et al. (2008) for several magnesio-riebeckite samples. Nevertheless, the UICC (Union for International Cancer Control) crocidolite standard is a riebeckite from South Africa that commonly contain higher Fe contents (Hodgson, 1979; Miyano and Beukes, 1997; Pacella et al., 2014). Bloise et al. (2016) investigated the thermal behavior of UICC crocidolite from Koegas Mine using thermo-gravimetry coupled with differential scanning calorimetry. Results obtained showed that the fibers decompose at around 850 °C with the formation of magnetite, cristobalite and acmite. Interestingly, despite the thermal treatment and the following change of the amphibole structure, the sample still preserves the fibrous habit (pseudomorphosis). Quantitative data on the percentage of the actual asbestos and the mineral species present as impurities in an UICC crocidolite standard sample are reported by Kohyama et al. (1986), showing a content of >99 wt% crocidolite and <1 wt% quartz. More recently, Della Ventura et al. (2018) indicated, in addition to quartz, the presence of very minor amounts of hematite, magnetite, talc, and lizardite for the same sample. Gualtieri et al. (2013) investigated the structural and microstructural changes of an UICC crocidolite standard sample after

injecting in mice peritoneum. Results indicated a partial fibre degradation of the crystalline structure following the incubation in the biological matrix. Rietveld refinement data highlighted intra-structure cation mobilization with Fe and Na migrating from site $M(2)$ to site $M(1)$ and from site $A(m)$ to site $M(4)$, respectively.

To clarify crocidolite structural details and define its cation distribution scheme, in the present work we carried out a full structural and spectroscopic characterization of an UICC crocidolite standard sample from Koegas Mine, Northern Cape (South Africa). Cation site partition, especially of $Fe^{2+}$ and $Fe^{3+}$ ionic species, was obtained from SEM-EDS chemical data integrated by $^{57}Fe$ Mössbauer spectroscopy and X-ray powder diffraction data.

## EXPERIMENTAL

### Scanning Electron Microscopy with Energy Dispersive System (SEM-EDS)

The micro-chemical characterization was performed using a Quanta 400 SEM (FEI, Hillsboro, Oregon, USA) equipped with an EDX Genesis EDS system. Operating conditions were: 15 kV accelerating voltage, 11 mm working distance, 0° tilt angle. SEM analysis was done on the flattened part of fibre bundles (6 analytical points) in order to avoid the effects due to particle geometry on the ability to obtain quantitative EDS data (Pacella et al., 2016; Newbury and Ritchie, 2013; Paoletti et al., 2011, 2008). In addition, analyses on dispersed fibers were performed and results confirmed the homogeneity of the fibre chemical composition (e.g. Ca absence). Table 1 shows the average chemical composition and crystal-chemical formula normalized on the basis of 24 O. Cations are reported in atoms per formula unit (apfu) and were assigned following Hawthorne et al. (2012). In addition, the morphology of the fibres was investigated by Field-Emission SEM Gemini 500.

### $^{57}Fe$ Mössbauer Spectroscopy

About 10 mg of UICC crocidolite were gently ground in an agate mortar with acetone and mixed with a powdered acrylic resin to avoid (or reduce) preferred orientations. The absorber was within the limits for the thin absorber thickness described by Long et al. (1983). Data were collected at room temperature and calibrated against both the 4-lines and 6-lines α-Fe spectra, using a conventional spectrometer system operated in constant acceleration mode, with a $^{57}Co$ source of nominal strength of 1850 MBq (50 mCi) in rhodium matrix, and recorded in a multichannel analyzer using 512 channels. After velocity calibration against a spectrum of high-purity α-iron foil (25 μm thick), the raw data were folded to 256 channels. The spectrum was fitted using Recoil 1.04 fitting program

Table 1. Chemical composition of the UICC crocidolite standard sample from SEM-EDX data

| Oxides | Wt% | | Cations on basis of 24 (O,OH,F) | |
|--------|-----|---|---------------------------------|---|
| $SiO_2$ | 52.37(19) | | Si | 7.950(18) |
| $Al_2O_3$ | 0.12(18) | T | Al | 0.022(32) |
| $Fe_2O_3$ | 17.87(32) | | total | **7.972(14)** |
| FeO | 17.42(31) | | $Fe^{3+}$ | 2.041(39) |
| MgO | 3.30(35) | | $Fe^{2+}$ | 2.212(43) |
| CaO | - | C | Mg | 0.747(77) |
| $Na_2O$ | 6.88(27) | | total | **5.000(5)** |
| $H_2O$ | 2.04 | | Na | 2.026(75) |
| Total | 100.00 | B | total | **2.026(75)** |

Note: Standard deviations are reported in brackets.

(Lagarec and Rancourt, 1988). Pure Lorentian line shape were fitted, and results were satisfactory. After a number of trials, a model based on five Lorentzian doublets, with three doublets for $Fe^{2+}$ and two doublets for $Fe^{3+}$, was chosen (Table 2). An alternative fitting strategy based on quadrupole splitting distributions was tested, and results were in agreement with those obtained using the Lorentzian approach (reduced $\chi^2$ between 1.0 and 1.5 and reasonable parameters, in line with the specific literature). The extended spectrum (6-lines calibration) revealed the presence of minor magnetic contribution to the absorption that was fitted with two magnetic sextets. Uncertainties were calculated using the covariance matrix and the errors were estimated to be approximately ±3% for both $Fe^{2+}$ and $Fe^{3+}$ absorption areas.

**X-ray Powder Diffraction (XRPD)**

X-ray powder diffraction data were collected on a Bruker AXS D8 Advance operating in θ/θ transmission mode. The powder was charged in a 0.5 mm diameter borosilicate glass capillary that was aligned on a standard goniometer stage. The instrument is fitted with an incident beam focussing Göbel mirror and a PSD VÅntec-1. Measurement was performed, using CuKα, in the 5-145° 2θ angular range, 0.022° 2θ step size and 10 s counting time. Data were evaluated by the Rietveld method using Topas V4.2 (Bruker AXS, 2009) applying the Fundamental Parameters Approach FPA (Cheary and Coelho, 1992). Owing to the strong correlations with site occupancies the structure of crocidolite was refined keeping fixed all displacement parameters to reference data, following the same approach used by Andreozzi et al. (2009). No restraints on bond distances and angles were imposed. Site scattering (*s.s.*) at $M(1)$, $M(2)$, $M(3)$ and $M(4)$ was optimized. Very low electron density was detected at A-type sites in keeping with the very small cationic excess at $M(4)$. For stabilizing the refinement, a single A site was used to model this behaviour. Careful scrutiny of the pattern revealed the occurrence of minor magnetite, calcite, quartz, siderite and minnesotaite. In particular, minnesotaite $(Fe^{2+},Mg)_3[Si_4O_{10}](OH)_2$ is a fairly common phyllosilicate pertaining to the pyrophyllite-talc group (Guggenheim and Eggleton, 1986) that has been reported as an accessory phase at the Koegas-Westerberg area (Cilliers et al., 1961). For the accessory phases, only scale factors, cell parameters and peak shapes were refined.

Peak broadening followed a Lorentzian (size) and a Gaussian (strain) behaviour (Delhez et al., 1993). The $\varepsilon_0$ microstrain (lattice strain), defined as $\beta_i=4e_0 \tan \theta$, and the volume-weighted mean column height $L_{vol}$, defined as $\beta_i=l/L_{vol} \cos \theta$ were extracted from the integral breadths $\beta b_i$ of the individual reflections (Ballirano and Sadun, 2009). Subsequently, an attempt to model a size-dependent anisotropic broadening of the reflections of crocidolite was carried out using the ellipsoid-model of Katerinopoulou et al. (2012) describing the diffraction-vector dependent broadening of diffraction maxima. In the monoclinic symmetry, the shape ellipsoid parameters $b_{ij}$ are constrained as $b_{11} \neq b_{22} \neq b_{33}$; $b_{12}=b_{23}=0$. An improvement

Table 2. Room temperature $^{57}$Mössbauer parameters of the UICC crocidolite standard sample.

| UICC crocidolite | δ | $\Delta E_Q$ | Γ | Assignment | Area (%) | $Fe^{3+}/Fe_{Tot}$ (raw) | $Fe^{3+}/Fe_{Tot}$ (corr) |
|------------------|---|--------------|---|------------|----------|--------------------------|---------------------------|
| | 1.14 | 2.88 | 0.32 | $^{VI}Fe^{2+}$ | 25 | | |
| | 1.14 | 2.39 | 0.36 | $^{VI}Fe^{2+}$ | 15 | | |
| | 1.08 | 2.23 | 0.76 | $^{VI}Fe^{2+}$ | 7 | 0.53 | 0.48 |
| | 0.40 | 0.44 | 0.28 | $^{VI}Fe^{3+}$ | 23 | | |
| | 0.33 | 0.00 | 1.50 | $^{VI}Fe^{3+}$ | 30 | | |

Note: Fit with Lorentzian doublets; temperature=298 K; δ=centre shift (with respect to an α-iron foil); $\Delta E_Q$=quadrupole splitting; Γ=full width at half maximum; Area=absorption area. Errors were estimated at about ±2 mm/s for δ, $\Delta E_Q$ and Γ, and no less than ±3% absolute for doublet areas.

PM

of the fit was observed as well as a reduction of standard deviations. Absorption was modelled following the approach of Sabine et al. (1998) for a cylindrical sample. Preferred orientation of crocidolite was modelled by means of spherical harmonics (nine refinable parameters up to the 4th order), resulting in a minor improvement of the fit, coherently with extremely small parameters, as expected for a capillary mount.

The Quantitative Phase Analysis (QPA) results are reported in Table 3, relevant parameters of the refinement, including statistical indicators, are listed in Table 4. Rietveld plots are shown in Figure 1. QPA follows the check list indicated in Gualtieri et al. (2019). Table 5 reports the relevant bond distances of crocidolite. The

corresponding CIF file of UICC crocidolite is available for downloading at the web site of the journal.

Table 3. Quantitative Phase Analysis of the UICC crocidolite standard sample.

| Phases | wt% | Reference structural data |
|---|---|---|
| Crocidolite | 93.67(19) | Hawthorne (1978) |
| Magnetite | 1.85(6) | Wechsler et al. (1984) |
| Quartz | 1.48(4) | Le Page and Donnay (1976) |
| Calcite | 1.30(9) | Ballirano (2011) |
| Siderite | 1.12(9) | Effenberger et al. (1981) |
| Minnesotaite | 0.57(6) | Guggenheim and Eggleton (1986) |

Table 4. Microstructural parameters of the UICC crocidolite standard sample (see text) and agreement factors (as defined in Young, 1993) of the Rietveld refinement. Isotropic and anisotropic refers to refinements carried out with an isotropic/anisotropic model of peak broadening (see text for details).

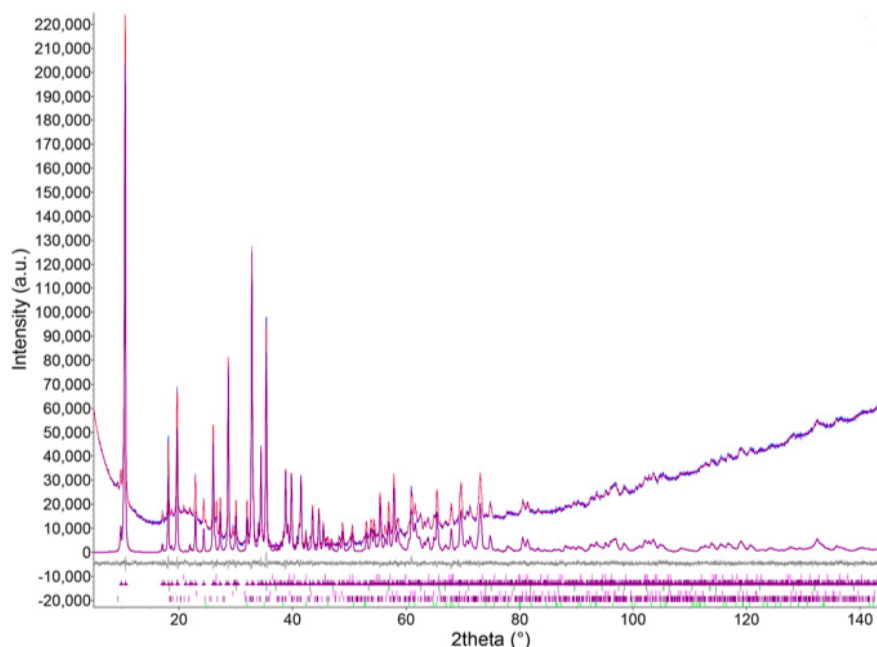| | isotropic | anisotropic |
|---|---|---|
| $L_{vol}$ (nm) | 63.9(15) | - |
| $b_{11}$ | - | 4.37(14) |
| $b_{22}$ | - | 0.56(4) |
| $b_{33}$ | - | 9.7(5) |
| $b_{13}$ | - | 3.57(19) |
| $\varepsilon_o$ | 0.040(5) | 0.0714(19) |
| $R_{Bragg}$ (%) | 0.86 | 0.70 |
| $R_{wp}$ (%) | 2.74 | 2.69 |
| $R_p$ (%) | 1.66 | 1.66 |
| GoF | 4.41 | 4.32 |
| DWd | 1.49 | 1.56 |



Figure 1. Rietveld plots of UICC crocidolite sample. Blue dotted line: experimental pattern; red continuous line: calculated; grey continuous line: difference plot; red continuous line calculated crocidolite contribution; vertical bars: position of the calculated Bragg reflections of, from above to below: quartz, crocidolite, magnetite, calcite, minnesotaite and siderite.

Table 5. Relevant bond distances (in Å) of the UICC crocidolite standard sample.

| | | | | | |
|---|---|---|---|---|---|
| $T(1)$ | -O(7) | 1.626(5) | $T(2)$ | -O(4) | 1.589(8) |
| | -O(6) | 1.629(6) | | -O(5) | 1.612(8) |
| | -O(1) | 1.632(10) | | -O(2) | 1.640(9) |
| | -O(5) | 1.635(9) | | -O(6) | 1.672(8) |
| $<T(1)-O>$ | | 1.630 | $<T(2)-O>$ | | 1.628 |
| | | | | | |
| $M(1)$ | -O(3) x2 | 2.083(7) | $M(2)$ | -O(4) x2 | 1.912(7) |
| | -O(1) x2 | 2.085(9) | | -O(2) x2 | 2.066(8) |
| | -O(2) x2 | 2.126(7) | | -O(1) x2 | 2.112(7) |
| $<M(1)-O>$ | | 2.098 | $<M(2)-O>$ | | 2.030 |
| | | | | | |
| $M(3)$ | -O(1) x4 | 2.116(7) | $M(4)$ | -O(4) x2 | 2.359(9) |
| | -O(3) x2 | 2.129(12) | | -O(2) x2 | 2.364(8) |
| $<M(3)-O>$ | | 2.120 | | -O(6) x2 | 2.513(8) |
| | | | | -O(5) x2 | 2.900(8) |
| $A$ | -O(7) x2 | 2.540(10) | $<M(4)-O>$ | | 2.534 |
| | -O(5) x4 | 2.887(7) | | | |
| | -O(6) x4 | 3.296(6) | | | |
| $<A-O>$ | | 2.981 | | | |

**RESULTS AND DISCUSSION**

The fibres of UICC crocidolite standard sample here examined appear straight, rigid and very tiny even when observed at high magnification through FE-SEM images. In addition, high-resolution images show that the micrometric fibres may split into smaller fibrils with diameter of ca. 0.1 µm (Figure 2).

The SEM-EDS analyses revealed substantial chemical homogeneity of the fibres (Table 1). Combining chemical data with Mössbauer results the following crystal-chemical formula was retrieved: $^{A}Na_{0.026}{}^{B}Na_{2.000}$ $^{C}(Fe^{2+}_{2.212}Fe^{3+}_{2.041}Mg_{0.747})_{\Sigma=5.000}{}^{T}(Si_{7.950}Al_{0.022})_{\Sigma=7.972}$ $O_{22}{}^{O(3)}(OH)_2$, fairly close to the end-member riebeckite, ideally $^{A}\square^{B}Na_2{}^{C}(Fe^{2+}{}_3Fe^{3+}{}_2)_{\Sigma=5}{}^{T}Si_8O_{22}{}^{O(3)}(OH)_2$.

The chemical composition of the investigated sample is closely comparable to those obtained on two UICC crocidolite standard samples coming from the same locality and previously studied by Pacella et al. (2014) $[^{A}\square^{B}(K_{0.01}Na_{1.64}Ca_{0.14}Mg_{0.16})_{\Sigma=1.95}{}^{C}(Fe^{2+}_{2.13}Fe^{3+}_{2.30}$ $Mg_{0.55}Mn_{0.01}Ti_{0.01})_{\Sigma=5.00}(Si_{7.82}Al_{0.02})_{\Sigma=7.84}O_{22}(OH)_{2.1}]$ and by Della Ventura et al. (2018) $[^{A}(K_{0.01}Na_{0.03})_{\Sigma=0.04}$ $^{B}(Ca_{0.04}Na_{1.96})_{\Sigma=2.00}{}^{C}(Fe^{2+}_{2.22}Fe^{3+}_{2.15}Mg_{0.52}Mn_{0.01})_{\Sigma=4.90}$ $(Si_{7.92}Al_{0.02})_{\Sigma=7.94}O_{22}(OH)_{2.2}]$, using Mössbauer data coupled with ICP-OES and SEM/EDS analysis, respectively. In detail, the main differences between the UICC crocidolite sample investigated in this work and the other two samples are the absence of Ca and a slightly lower $Fe_{tot}$ content.

The room temperature $^{57}Fe$ Mössbauer spectrum of the investigated UICC crocidolite sample calibrated against the 4-lines α-Fe spectrum shows two main absorptions between -1 and 3 mm/s (Figure 3a). The crocidolite spectrum is well comparable with literature spectra collected on UICC crocidolite (Stroink et al., 1980) and on riebeckite (Susta et al., 2018). The presence of very weak absorption in the external part of the spectrum raised the suspect of a magnetic contribution from Fe oxides/hydroxides, possibly due to accessory phases and/or surface alteration. The crocidolite extended spectrum (calibrated against the 6-lines α-Fe spectrum) confirmed the presence of a magnetic Fe oxide that was identified as magnetite, with two sextets characterized by centre shift δ=0.23 and 0.66 mm/s, magnetic field H=48.87 and 46.07 Tesla, and absorption area ~3 and 7% $Fe_{Tot}$, respectively (Figure 3b). The absorption contribution of the two magnetic sextets accounts for ~10 % of the total Fe, which allows quantifying the magnetite as ~3 wt% of the UICC crocidolite standard sample. Apart from the magnetite contribution, the experimental Mössbauer absorption
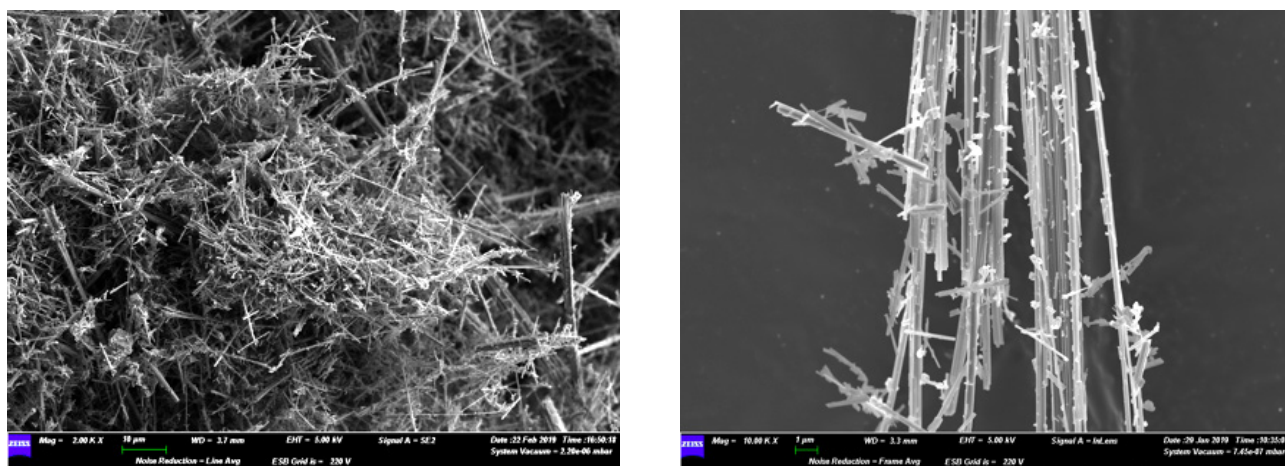
Figure 2. FE-SEM images of UICC crocidolite fibres at increasing magnification clearly showing single fibrils coming from the splitting of micrometric fibres.
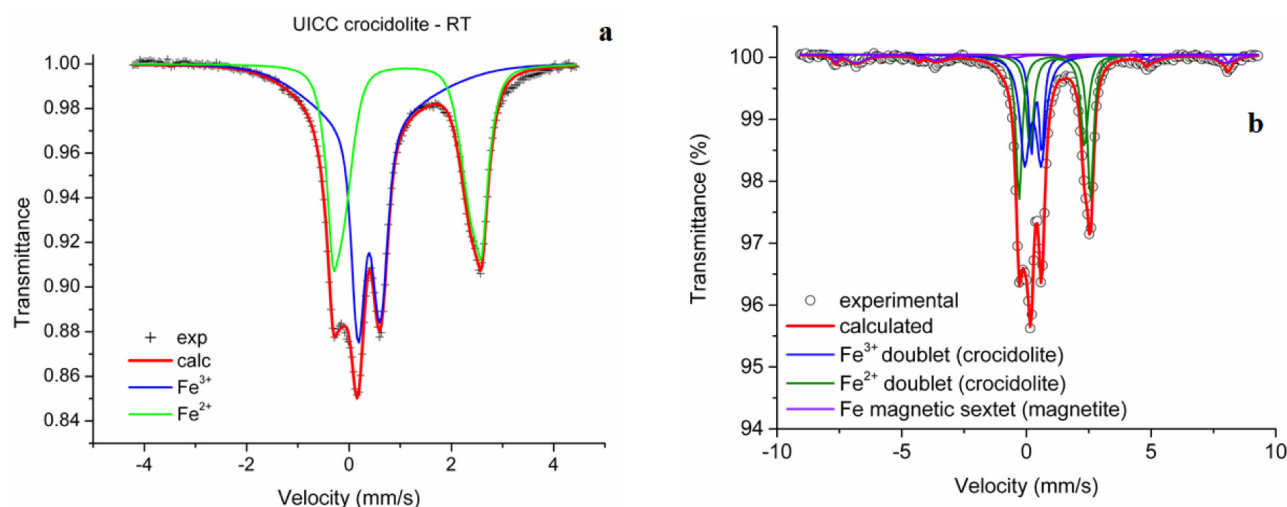


Figure 3. Room temperature $^{57}$Fe Mössbauer spectrum of the UICC crocidolite sample: a) spectrum calibrated against the 4-lines α-Fe spectrum (fit with Quadrupole Splitting Distribution); b) extended spectrum, calibrated against the 6-lines α-Fe spectrum, showing the magnetite contribution (fit with pure Lorentzian lines).

spectrum of crocidolite was reproduced by the convolution of five doublets representing $Fe^{2+}$ and $Fe^{3+}$ ionic species in octahedral coordination (Table 2). In particular, $Fe^{2+}$ contribution was modelled by three doublets with almost constant centre shift (δ values close to 1.1 mm/s) and clearly distinguished quadrupole splitting (ΔE$_Q$) values: 2.9, 2.4 and 2.2 mm/s. These data are in agreement with the existing literature and are interpreted as representing $Fe^{2+}$ at octahedrally-coordinated sites with different next-nearest neighbour coordination environments. The contribution of $Fe^{3+}$ was modelled by two components with comparable δ of 0.3-0.4 mm/s and distinguished by ΔE$_Q$ of 0 and 0.4 mm/s. The $Fe^{3+}$/Fe$_{Tot}$ ratio was quantified on the basis of spectral area measurement (and reported

in the "raw" column in Table 3), later corrected for the temperature effect ("corr" column in Table 3) applying the empirical correction factor of Dyar et al. (1993). The corrected $Fe^{3+}$/Fe$_{tot}$ ratio obtained for UICC crocidolite is 0.48, which suggests that this sample is slightly more oxidized than the end-member riebeckite (ideal ratio of 0.40).

Refined UICC crocidolite cell parameters are $a$=9.73516(19) Å, $b$=18.0453(3) Å, $c$=5.32895(9) Å, β =103.5159(12) °, $V$=910.23(3) Å$^3$. The QPA indicates that 93.7(3) wt.% of the sample consists of crocidolite, the remaining being distributed among five different phases, the relatively most abundant of which is the magnetite, quantified at ~2 wt% (Table 3). Results here obtained are

only in partial agreement with the findings of Kohyama et al. (1986), who reported, for the same sample, a content of >99 wt% crocidolite and <1 wt% quartz.

Structural details of the UICC crocidolite standard sample here examined are compared with those reported by Gualtieri et al. (2013) for the same material and Susta et al. (2018) for riebeckite in Table 6. The results of the present refinement are very close to those of Susta et al. (2018) as the mean bond distances differ of <0.01 Å with the only exception of $<M(1)-O>$ whose difference is of 0.020 Å, likely due to slightly different chemical composition of the two samples. Larger differences are observed with respect to data reported by Gualtieri et al. (2013), in particular with respect to the $<M(3)-O>$ bond distance (that was reported to be 2.217 Å, a value anomalously large). The observed discrepancy may be attributed, as pointed out by the authors, to the significant

contribution to the diffraction pattern of the components used for sample preparation, which affected the accuracy of the structural data.

The refined site scattering (*s.s.*) at C group sites (120.2(8) e⁻) is in excellent agreement with that from combined chemical and Mössbauer data (119(3) e⁻), as reported in Table 7. Following the approach of Vignaroli et al. (2014), an indirect $Fe^{2+}/Fe^{3+}$ partition was performed by comparing the $<r^M>$ mean cationic radii calculated from both the refined $<M(1,2,3)-O>$ bond distances and from the proposed site partition. The $<r^M>$ were calculated following the conventional assignment to the C group sites (Hawthorne, 1981) and using the cation ionic radii taken from Shannon (1976) by considering an $^{III}O$ radius of 1.36 Å (Table 7). The result of this process produces a $Fe^{2+}/Fe^{3+}=1.07$, which is in very good agreement with 1.08(4) obtained combining chemical and Mössbauer

Table 6. Comparison of mean bond distances (in Å) of the UICC crocidolite standard sample with reference data.

| Mean bond distances | UICC crocidolite (present work) | Gualtieri et al. (2013) | Susta et al. (2018)* |
|---|---|---|---|
| $<T(1)-O>$ | 1.630 | 1.650 | 1.625 |
| $<T(2)-O>$ | 1.628 | 1.631 | 1.632 |
| $<M(1)-O>$ | 2.098 | 2.086 | 2.118 |
| $<M(2)-O>$ | 2.030 | 2.068 | 2.031 |
| $<M(3)-O>$ | 2.120 | 2.217 | 2.123 |
| $<M(4)-O>$ | 2.534 | 2.498 | 2.541 |

Note: *Data of Susta et al. (2018) refer to riebeckite.

Table 7. Crystal chemistry of the UICC crocidolite standard sample. Left side: experimental site scattering (exp. *s.s.*) at C sites from Rietveld refinement, Mg-Fe partition from *s.s.*, $Fe^{2+}$-$Fe^{3+}$ partition from $<r^M>$. Right side: calculated site scattering (calc. *s.s.*) from chemical formula, $Fe^{2+}$-$Fe^{3+}$ partition from combined SEM-EDX and Mössbauer data.

| Site | exp. *s.s.*(e⁻) | Mg-Fe partition from *s.s.* | $Fe^{2+}$-$Fe^{3+}$ partition from $<r^M>$ | calc. *s.s.* (e⁻) | $Fe^{2+}$-$Fe^{3+}$ partition from SEM and Mössbauer data |
|---|---|---|---|---|---|
| T | | | | | $[Si_{7.95(2)}Al_{0.02(3)}]$ |
| C | | | | | |
| $M(1)$ | 45.4(2) | $Mg_{0.47}Fe_{1.53(2)}$ | $[Mg_{0.47}Fe^{3+}_{0.41}Fe^{2+}_{1.12}]$ | | $[Mg_{0.50}Fe^{3+}_{0.31}Fe^{2+}_{1.19}]$ |
| $M(2)$ | 50.6(3) | $Mg_{0.10}Fe_{1.90(1)}$ | $[Mg_{0.10}Fe^{3+}_{1.58}Fe^{2+}_{0.32}]$ | | $[Mg_{0.10}Fe^{3+}_{1.60}Fe^{2+}_{0.30}]$ |
| $M(3)$ | 24.2(3) | $Mg_{0.13}Fe_{0.87(1)}$ | $[Mg_{0.13}Fe^{3+}_{0.09}Fe^{2+}_{0.78}]$ | | $[Mg_{0.15}Fe^{3+}_{0.13}Fe^{2+}_{0.72}]$ |
| $S_{M(1)+M(2)+M(3)}$ | **120.2(8)** | **$Mg_{0.70}Fe_{4.30(4)}$** | **$[Mg_{0.70}Fe^{3+}_{2.08}Fe^{2+}_{2.22}]$** | **119(3)** | **$[Mg_{0.75(8)}Fe^{3+}_{2.04(4)}Fe^{2+}_{2.21(4)}]$** |
| $Fe^{2+}/Fe^{3+}$ | | | 1.07 | | 1.08(4) |
| B | | | | | |
| $M(4)$ | 20.8(2) | $Na_{1.89(1)}$ | $Na_{1.89}$ | | $Na_{2.00(7)}$ |
| *Am* | 0.6(3) | $Na_{0.05(2)}$ | $Na_{0.05(2)}$ | | $Na_{0.03(7)}$ |

data. According to this procedure, the UICC crocidolite sample allocates $Fe^{3+}$ with the following site-preference sequence $M(2)>>M(1)>M(3)$ and $Fe^{2+}$ with the sequence $M(3)>M(1)>>M(2)$. As a result, the final partition here proposed is:

$[Mg_{0.50}Fe^{3+}_{0.31}Fe^{2+}_{1.19}]_{\Sigma=2.00}$ at $M(1)$;
$[Mg_{0.10}Fe^{3+}_{1.60}Fe^{2+}_{0.30}]_{\Sigma=2.00}$ at $M(2)$;
$[Mg_{0.15}Fe^{3+}_{0.13}Fe^{2+}_{0.72}]_{\Sigma=1.00}$ at $M(3)$.

Comparison between measured and calculated $<r^M>$ mean cationic radii shows an excellent agreement, with discrepancies ranging within one standard deviation of $M$-O bond distances.

## CONCLUSIONS

This work reports an accurate crystal-chemical characterization of the UICC crocidolite standard sample coming from Koegas Mine, Northern Cape (South Africa) obtained using a multi-analytical chemical, spectroscopic and diffractometric approach. The chemical formula and the cation distribution, obtained on the basis of a combination of all data, showed that the investigated sample is very close to the riebeckite end member.

Although the UICC crocidolite standard reference has been extensively used for toxicological investigations, an accurate, full crystal structural characterization of the fibres was still missing. Our QPA revealed the presence of about 7 wt% of accessory phases, much more than those observed by Kohyama et al. (1986) and Della Ventura et al. (2018), highlighting the occurrence of non-negligible contents of impurities in the UICC crocidolite standard samples. Notably, the presence of quartz, a mineral of well know toxic potential, and Fe-bearing phases such as magnetite and minor siderite and minnesotaite, is a relevant aspect to be taken in due consideration in case of reactivity and toxicity studies on UICC crocidolite fibres.

## REFERENCES

Andreozzi G.B., Ballirano P., Gianfagna A., Mazziotti-Tagliani S., Pacella A., 2009. Structural and spectroscopic characterization of a suite of fibrous amphiboles with high environmental and health relevance from Biancavilla (Sicily, Italy). American Mineralogist 94, 1333-1340.

Andreozzi G.B., Pacella A., Corazzari I., Tomatis M., Turci, F., 2017. Surface reactivity of amphibole asbestos: a comparison between crocidolite and tremolite. Scientific Reports 7, 14696.

Ballirano P., 2011. Laboratory parallel-beam transmission X-ray powder diffraction investigation of the thermal behavior of calcite: comparison with X-ray single-crystal and synchrotron powder diffraction data. Periodico di Mineralogia 80, 123-134.

Ballirano P. and Sadun C., 2009. Thermal behavior of trehalose dihydrate (Th) and β-anhydrous trehalose (Tβ) by in-situ laboratory parallel-beam X-ray powder diffraction. Structural Chemistry 20, 815-823.

Bloise A., Catalano M., Barrese E., Gualtieri A.F., Bursi Gandolfi N., Capella S., and Belluso E., 2016. TG/DSC study of the thermal behaviour of hazardous mineral fibres. Journal of Thermal Analysis and Calorimetry 123, 2225-2239.

Bonneau L., Malard C., Pezerat H., 1986. Studies on surface properties of asbestos. 2. Role of dimensional characteristics and surface properties of mineral fibers in the induction of pleural tumors. Environmental Research, 41, 268-275.

Bruker AXS, 2009. Topas V4.2: General profile and structure analysis software for powder diffraction data. Bruker AXS, Karlsruhe, Germany.

Cheary R.W. and Coelho, A., 1992. A fundamental parameters approach to X-ray line-profile fitting. Journal of Applied Crystallography 25, 109-121.

Cilliers J.J. Le R., Freeman A.G., Hodgson A., Taylor H.F.W., 1961. Crocidolite from the Koegas-Westerberg area, South Africa. Economic Geology 56, 1421-1437.

Delhez R., de Keijser T.H., Langford J.I., Louër D., Mittemeijer E.J., Sonneveld E.J., 1993. Crystal imperfection broadening and peak shape in the Rietveld method: In: Young R.A. (Ed.) "The Rietveld method". Oxford University Press, 132-166.

Della Ventura G, Vigliaturo R., Gieré R., Pollastri S., Gualtieri A.F, Iezzi G., 2018. Infra Red Spectroscopy of the Regulated Asbestos Amphiboles. Minerals, 8(9), 413; https://doi.org/10.3390/min8090413.

Dyar M.D., Mackwell S.M., McGuire A.V., Cross L.R., Robertson J.D., 1993. Crystal chemistry of Fe3+ and H+ in mantle kaersutite: implications for mantle metasomatism. American Mineralogist 78, 968-979.

Effenberger H., Mereiter K., Zemann J., 1981. Crystal structure refinements of Magnesite, Calcite, Rhodochrosite, Siderite, Smithonite, and Dolomite, with the discussion of some aspects of the stereochemistry of Calcite type carbonates. Zeitschrift für Kristallographie 156, 233-243.

Favero-Longo S.E., Castelli D., Salvadori O., Belluso E., Piervittori R., 2005. Pedogenetic action of the lichens Lecidea atrobrunnea, Rhizocarpon geographicum gr. and Sporastatia testudinea on serpentinized ultramafic rocks in an alpine environment. International Biodeterioration and Biodegradation 56, 17-27.

Fubini B., 1993. The possible role of surface chemistry in the toxicity of inhaled fibers. In: Wahreit D.B. (Ed.), Fiber Toxicology, 11. Academic Press, San Diego, 229-257.

Fubini B. and Mollo L., 1995. Role of iron in the reactivity of mineral fibers. Toxicology Letters 82-83, 951-960.

Fubini B., 1996. Physico-chemical and cell free assays to evaluate the potential carcinogenicity of fibres. In: Kane A.B., Boffetta P., Saracci R., Wilbourn J. (Eds.), Mechanisms of Fibre Carcinogenesis. IARC Scientific Publication, Lyon, 140.

Gazzano E., Riganti C., Tomatis M., Turci F., Bosia A., Fubini B., Ghigo D., 2005. Potential toxicity of nonregulated asbestiform minerals: balangeroite from the western Alps. Part 3: depletion of antioxidant defenses. Journal of Toxicology and Environmental Health 68, 41-49.

Gilmour P.S., Brown D.M., Beswik P.H., Macnee W., Rahman I., Donaldson K., 1997. Free radical activity of industrial fibers: role of iron in oxidative stress and activation of transcription factors. Environmental Health Perspectives, 105 (Suppl. 5), 1313-1317.

Gualtieri A.F, Gatta G.D., Arletti R., Artioli G., Ballirano P., Cruciani G., Guagliardi A., Malferrari D., Masciocchi N., Scardi P., 2019. Quantitative phase analysis using the Rietveld method: toward a procedure for checking the reliability and quality of the results. Periodico di Mineralogia 88, 147-151.

Gualtieri A.F., Giacobbe C., Rinaudo C., Croce A., Allegrina M., Gaudino G., Yang H., Carbone M., 2013. Preliminary results of the spectroscopic and structural characterization of mesothelioma inducing crocidolite fibers injected in mice. Periodico di Mineralogia 82, 299-312.

Guggenheim S. and Eggleton R.A., 1986. Structural modulations in iron-rich and magnesium-rich minnesotaite. Canadian Mineralogist 24, 479-497.

Hawthorne F.C., 1978. The crystal chemistry of the amphiboles. VIII. The crystal structure and site chemistry of fluor-riebeckite. Canadian Mineralogist 16, 187-194.

Hawthorne, F.C., 1981. Crystal chemistry of the amphiboles. In D.R. Veblen Ed., Amphiboles and other hydrous pyriboles Mineralogy, pp. 1-102, Reviews in Mineralogy 9A, Mineralogical Society of America.

Hawthorne F.C., Oberti R., Zanetti A., Nayak V.K., 2008. The crystal chemistry of alkali amphiboles from the Kajlidongri manganese mine, India. Canadian Mineralogist 46, 455-466.

Hawthorne F.C., Oberti R., Harlow G.E., Maresch W.V., Martin R.F., Schumacher J.C., Welch M.D., 2012. Nomenclature of the amphibole supergroup. American Mineralogist 97, 2031-2048.

Hodgson A.A., 1979. Chemistry and physics of asbestos. In: Michaels L. and Chissick S.S. (Eds.) "Asbestos - Properties, Applications and Hazards. John Wiley & Sons, New York, 67-114.

International Agency for Research on Cancer (IARC), 2012. In Arsenic, metals, fibres, and dusts Vol. 100C Monographs on the evaluation of carcinogenic risks to humans, 219-309.

Katerinopoulou A., Balic-Zunic T., Lundegaard L.F., 2012. Application of the ellipsoid modeling of the average shape of nanosized crystallites in powder diffraction. Journal of Applied Crystallography 45, 22-27.

Kohyama N., Shinohara Y., Suzuki Y., 1996. Mineral phases and some reexamined characteristics of the International Union against cancer standard asbestos samples. American Journal of Industrial Medicine 30, 515-528.

Lagarec K. and Rancourt D.G., 1998. RECOIL. Mössbauer spectral analysis software for Windows, version 1.0. Department of Physics, University of Ottawa, Canada.

Le Page Y. and Donnay G., 1976. Refinement of the crystal structure of low-quartz. Acta Crystallographica B32, 2456-2459.

Long G.J., Cranshaw T.E., Longworth G., 1983. The ideal Mössbauer effect absorber thickness. Mössbauer Effect Reference Data Journal 6, 42-49.

Martra G., Tomatis M., Fenoglio I., Coluccia S., and Fubini B., 2003. Ascorbic acid modifies the surface of asbestos: possible implicationsin the molecular mechanisms of toxicity. Chemical Research in Toxicology 16, 328-335.

Miyano T. and Beukes N.J., 1997. Mineralogy and petrology of the contact metamorphosed amphibole asbestos-bearing Penge iron formation, Eastern Transvaal, South Africa. Journal of Petrology 5, 651-676.

Newbury D.E. and Ritchie N.W., 2013. Is scanning electron microscopy/energy dispersive X-ray spectrometry (SEM/EDS) quantitative? Scanning 35, 141-168.

Pacella A., Ballirano P., Cametti G., 2016. Quantitative chemical analysis of erionite fibres using a micro-analytical SEM-EDX method. European Journal of Mineralogy 28, 257-264.

Pacella A., Fantauzzi M., Turci F., Cremisin, C., Montereali M.R., Nardi E., Atzei D., Rossi A., Andreozzi G.B., 2014. Dissolution reactions and surface iron speciation of UICC crocidolite in buffered solutions at pH 7.4: a combined ICP-OES, XPS and TEM investigation. Geochimica et Cosmochimica Acta 127, 221-232.

Paoletti L., Bruni B.M., Arrizza L., Mazziotti-Tagliani S., Pacella A., 2008. A micro-analytical SEM-EDS method applied to the quantitative chemical compositions of fibrous amphiboles. Periodico di Mineralogia 77, 63-73.

Paoletti L., Bruni B.M., Gianfagna A., Mazziotti-Tagliani S., Pacella A., 2011. Quantitative Energy Dispersive X-ray analysis of sub-micrometric particles using a Scanning Electron Microscope. Microscopy and microanalysis 17, 710-717.

Sabine T.M., Hunter B.A., Sabine W.R., Ball C.J., 1998. Analytical expressions for the transmission factor and peak shift in absorbing cylindrical specimens. Journal of Applied Crystallography 31, 47-51.

Shannon R.D., 1976. Revised effective ionic radii and systematic studies of interatomic distances in halides and chalcogenides. Acta Crystallographica A 32, 751-767.

Stanton M.F., Layard M., Tegeris A., Miller E., May M., Morgan E., Smith A., 1981. Relation of particle dimension to carcinogenicity in amphibole asbestoses and other fibrous minerals. Journal of the National Cancer Institute 67, 965-975.

Stroink G., Blaauw C., White C.G., Leiper W., 1980. Mössbauer characteristics of UICC standard reference asbestos samples. Canadian Mineralogist 18, 285-290.

Susta U., Della Ventura G., Hawthorne F.C., Abdu Y.A., Day M.C., Mihailova B., Oberti R., 2018. The crystal-chemistry of riebeckite, ideally $Na_2Fe^{2+}3Fe^{3+}2Si_8O_{22}(OH)_2$: a multi-technique study. Mineralogical Magazine 82, 837-852.

Vignaroli G., Ballirano P., Belardi G., Rossetti F., 2014. Asbestos fibre identification vs. evaluation of asbestos hazard in ophiolitic rock mélanges, a case study from the Ligurian Alps (Italy). Environmental Earth Sciences 72, 3679-3698.

Wechsler B.A., Lindsley D.H., Prewitt C.T., 1984. Crystal structure and cation distribution in titanomagnetites $Fe_{3-x}Ti_xO_4$. American Mineralogist 69, 754-770.

Whittaker E.J.W., 1949. The structure of Bolivian crocidolite. Acta Crystallographica 2, 312-317.

Young R.A., 1993. Introduction to the Rietveld method: In: Young R.A. (Ed.) "The Rietveld method". Oxford University Press, 1-38.